

# Beyond Parameter Arithmetic: Sparse Complementary Fusion for Distribution-Aware Model Merging

Wei hong Lin<sup>1</sup> Lin Sun<sup>1</sup> Qilong Shi<sup>2</sup> Aomu fei Yuan<sup>2</sup> Yuxuan Tian<sup>2</sup> Zheng yang Wang<sup>2</sup> Guangxiang Zhao<sup>1</sup>  
Xiang zheng Zhang<sup>1</sup> Tong Yang<sup>2</sup>

## Abstract

Model merging has emerged as a promising paradigm for composing the capabilities of large language models by directly operating in weight space, enabling the integration of specialized models without costly retraining. However, existing merging methods largely rely on parameter-space heuristics, which often introduce severe interference, leading to degraded generalization and unstable generation behaviors such as repetition and incoherent outputs. In this work, we propose Sparse Complementary Fusion with reverse KL (SCF-RKL), a novel model merging framework that explicitly controls functional interference through sparse, distribution-aware updates. Instead of assuming linear additivity in parameter space, SCF-RKL measures the functional divergence between models using reverse Kullback-Leibler divergence and selectively incorporates complementary parameters. This mode-seeking, sparsity-inducing design effectively preserves stable representations while integrating new capabilities. We evaluate SCF-RKL across a wide range of model scales and architectures, covering both reasoning-focused and instruction-tuned models. Extensive experiments on 24 benchmarks spanning advanced reasoning, general reasoning and knowledge, instruction following, and safety demonstrate, vision classification that SCF-RKL consistently outperforms existing model merging methods while maintaining strong generalization and generation stability.

## 1. Introduction

Large language models (LLMs) have been demonstrating unprecedented capabilities across a wide spectrum of tasks,

<sup>1</sup>Beijing Qiyuan Technology Co., Ltd., Beijing, China <sup>2</sup>Peking University, Beijing, China. Correspondence to: Lin Sun <[sunlin1@360.cn](mailto:sunlin1@360.cn)>.

Preprint. February 13, 2026.

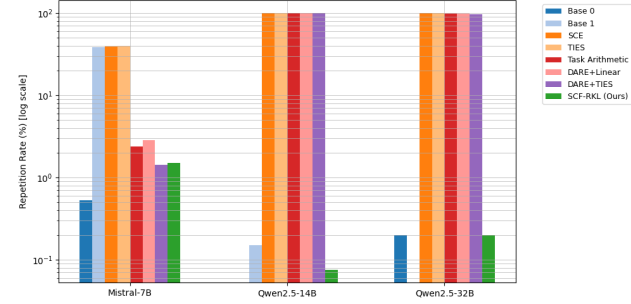


Figure 1. Repetition rates across fusion methods on Mistral-7B, Qwen2.5-14B, and Qwen2.5-32B. Baseline merging methods severely amplify repetition even when base models exhibit near-zero rates, whereas SCF-RKL consistently maintains low repetition (<1.6%) across all scales.

**Question:** Every day, Wendi feeds each of her chickens three cups of mixed chicken feed, containing seeds, mealworms and vegetables to help keep them healthy. She gives the chickens their feed in three separate meals. In the morning, she gives her flock of chickens 15 cups of feed. In the afternoon, she gives her chickens another 25 cups of feed. How many cups of food does she need to give her chickens in the final meal of the day if the size of Wendi's flock is 20 chickens?

chickens in the final meal of the day. Hmmm, let's start by understanding the problem step by step.... Subtracting the amount already given from the total required gives:  $60 \text{ cups} - 40 \text{ cups} = 20 \text{ cups}$ . **\*\*Answer:\*\*** Wendi needs to give her chickens 1 box of 20 cups of feed in the final meal.

**Question:** Which statement is accurate? (A) Yeah, I've noticed he's been drinking overly recently, and he's been acting really weird. (B) Yeah, he's been having a really bad time lately, and it's been causing him to feel really bad about his health or well-being. (C) Yeah, he's been having a really bad time lately, and it's been causing him to feel really bad about his health or well-being. (D) Yeah, he's been having a really bad time lately, and it's been causing him to feel really bad about his health or well-being. (E) Yeah, he's been having a really bad time lately, and it's been causing him to feel really bad about his health or well-being.

**Answer:** D. Yeah, he's been having a really bad time lately, and it's been causing him to feel really bad about his health or well-being. - Wrong to think (A) is correct because it's not a good statement. - Wrong to think (B) is correct because it's not a good statement. - Wrong to think (C) is correct because it's not a good statement. - Wrong to think (E) is correct because it's not a good statement.

**Explanation:** (A) is inaccurate because it's not a good statement. (B) is inaccurate because it's not a good statement. (C) is inaccurate because it's not a good statement. (E) is inaccurate because it's not a good statement.

**Question:** Which statement is accurate? (A) Yeah, I've noticed he's been drinking overly recently, and he's been acting really weird. (B) Yeah, he's been having a really bad time lately, and it's been causing him to feel really bad about his health or well-being. (C) Yeah, he's been having a really bad time lately, and it's been causing him to feel really bad about his health or well-being. (D) Yeah, he's been having a really bad time lately, and it's been causing him to feel really bad about his health or well-being. (E) Yeah, he's been having a really bad time lately, and it's been causing him to feel really bad about his health or well-being.

**Answer:** C. Yeah, he's been having a really bad time lately, and it's been causing him to feel really bad about his health or well-being. - Wrong to think (A) is correct because it's not a good statement. - Wrong to think (B) is correct because it's not a good statement. - Wrong to think (D) is correct because it's not a good statement.

**Explanation:** (A) is inaccurate because it's not a good statement. (B) is inaccurate because it's not a good statement. (D) is inaccurate because it's not a good statement.

**Question:** Which statement is accurate? (A) Yeah, I've noticed he's been drinking overly recently, and he's been acting really weird. (B) Yeah, he's been having a really bad time lately, and it's been causing him to feel really bad about his health or well-being. (C) Yeah, he's been having a really bad time lately, and it's been causing him to feel really bad about his health or well-being. (D) Yeah, he's been having a really bad time lately, and it's been causing him to feel really bad about his health or well-being. (E) Yeah, he's been having a really bad time lately, and it's been causing him to feel really bad about his health or well-being.

**Answer:** D. Yeah, he's been having a really bad time lately, and it's been causing him to feel really bad about his health or well-being. - Wrong to think (A) is correct because it's not a good statement. - Wrong to think (B) is correct because it's not a good statement. - Wrong to think (C) is correct because it's not a good statement.

**Explanation:** (A) is inaccurate because it's not a good statement. (B) is inaccurate because it's not a good statement. (C) is inaccurate because it's not a good statement.

Figure 2. Unstable generation in existing fusion: (Left) catastrophic repetition and (Right) incoherent outputs—whereas SCF-RKL preserves both correctness and coherence.

fostering a rapidly growing ecosystem of specialized models (e.g., Deepseek-R1(Guo et al., 2025), Qwen2.5(Qwen Team, 2024), Qwen3(Qwen Team, 2025), LLaMA3(Meta AI, 2024) , Mistral(Jiang et al., 2023) ) fine-tuned for reasoning(Wei et al., 2022), instruction following(Wang et al., 2025), safety alignment(Si et al., 2026; Tan et al., 2026), and domain-specific expertise. Model merging(Ilharco et al., 2022; Yadav et al., 2023; Du et al., 2024; Yang et al., 2023; Wan et al., 2025; Zeng et al., 2025; Chen et al., 2025; Ma et al., 2025) has recently emerged as a promising paradigm to integrate such complementary capabilities directly in weight space, offering a training-free alternative to costly retraining or continual finetuning. By composing pretrained or finetuned models, model merging enables practitioners to flexibly construct multi-capability systems, not only from publicly available open-source models, but also from custom-trained domain specialists(Sun et al., 2025).

While prior work reports promising gains on downstream benchmarks, a fundamental question remains underexplored:

**how stable is the generation behavior of merged models over long horizons?** In practice, many classical merging methods, including Task Arithmetic, TIES, DARE, and SCE, exhibit severe generation instabilities even when base models have near-zero repetition. As shown in Figure 1, these methods can drastically amplify repetition, often approaching 100% across model scales. Qualitatively, this instability manifests as degenerate repetition loops and semantically incoherent outputs, as illustrated in Figure 2. Such instabilities are especially damaging for long-form generation and multi-step reasoning, where small distributional distortions compound over time. Together, these observations expose a critical challenge: **can model merging integrate complementary capabilities while preserving long-horizon generation stability?**

**Our Approach.** We argue that generation failures in existing merging methods stem from a fundamental limitation: dense parameter-space fusion distorts the base model’s output distribution, causing entropy collapse and self-reinforcing token selection. We introduce Sparse Complementary Fusion with reverse KL (SCF-RKL), a distribution-aware framework that selectively integrates complementary parameters using reverse Kullback-Leibler divergence (Bishop & Nasrabadi, 2006) while enforcing sparsity to preserve generation stability. We evaluate SCF-RKL on 24 benchmarks across model scales (7B–32B) and architectures (Qwen2.5, LLaMA3, Mistral). Results show SCF-RKL consistently enhances reasoning and generalization, strongly suppresses degenerative repetition, maintains strong-model performance in asymmetric fusion, simultaneously improves reasoning and safety when integrating specialized models, and extends effectively to vision tasks, where it exhibits robust cross-modal generalization.

**Contributions.** First, we identify how existing methods amplify low-probability repetition behaviors, causing severe degradation. Second, we propose SCF-RKL, a principled sparse fusion framework using reverse KL divergence to preserve high-confidence components while avoiding repetition amplification. Third, we provide theoretical analysis showing reverse-KL-guided sparse fusion suppresses mode collapse with stronger stability guarantees than parameter averaging. Fourth, we demonstrate consistent empirical gains across 24 benchmarks in multiple fusion scenarios. Finally, we show SCF-RKL preserves model capacity ceilings and often surpasses both the strongest base model and existing baselines.

## 2. Sparse Complementary Fusion With Reverse KL

We propose Sparse Complementary Fusion with Reverse KL (SCF-RKL), a model merging framework that uses reverse KL divergence to selectively integrate complementary

expertise from domain-specialized models. By formulating fusion as sparse updates, SCF-RKL preserves base-model coherence while substantially reducing degeneration such as repetition and garbled outputs.

### 2.1. Problem Formulation

Let  $\theta_0 \in \mathbb{R}^d$  denote the parameters of a base model and  $\theta_1 \in \mathbb{R}^d$  those of a complementary model trained or specialized under different objectives (e.g., reasoning, instruction-following, or safety alignment). Our goal is to construct a fused model  $\theta_f$  that selectively incorporates the strengths of  $\theta_1$  while maintaining the stable generative behavior of  $\theta_0$ .

We define the fused parameters as:

$$\theta_f = \theta_0 + M \odot (\theta_1 - \theta_0)$$

where  $M \in \{0, 1\}^d$  is a sparse fusion mask that determines which parameters are updated.

The **central challenge** is to design  $M \in \{0, 1\}^d$  such that: (1) Only **informationally meaningful** updates are injected; (2) The fusion avoids large-scale parameter drift that leads to **mode collapse or repetitive generation**.

### 2.2. Importance Estimation via Reverse KL Divergence

**Parameter Distributions** For each parameter group (e.g., per output channel or hidden dimension), we interpret parameters as defining a categorical distribution via softmax:

$$p = \text{softmax}(\theta_1), \quad q = \text{softmax}(\theta_0)$$

where  $p$  and  $q$  represent the induced probability distributions of the complementary and base models, respectively.

**Reverse KL as an Information-Sensitive Metric** We measure the informational discrepancy between the two models using the **reverse Kullback–Leibler divergence**:

$$\text{RKL}(q \parallel p) = \sum_i q_i \log \frac{q_i}{p_i}$$

Unlike the forward KL divergence, which emphasizes covering the modes of  $p$ , reverse KL penalizes deviations that significantly alter regions of high probability under the base model. This property makes reverse KL particularly suitable for conservative fusion, as it prioritizes preserving the base model’s dominant probability mass.

**Information-theoretic Saliency Measure** Guided by the reverse KL divergence, we compute an information-theoretic saliency score for parameter selection:

$$I = |\theta_1 - \theta_0| \cdot \text{RKL}(q \parallel p)$$

This formulation couples **parameter deviation magnitude** with **information-geometric impact**, ensuring that large but informationally insignificant updates are suppressed.

### 2.3. Dynamic Sparse Complementary Fusion

To determine which parameters should be updated, we adopt a **distribution-adaptive thresholding strategy**.

Let  $I$  denote the set of all information-theoretic saliency score. We compute the median  $\text{med}(I)$  and the interquartile range  $\text{IQR}(I) = Q_{\text{high}}(I) - Q_{\text{low}}(I)$ . The fusion threshold is defined as:

$$\tau = \text{med}(I) + \alpha \cdot \text{IQR}(I)$$

where  $\alpha$  is a scale factor of  $\text{IQR}$ . The fusion mask is then:

$$M_i = \mathbb{I}[I_i \geq \tau]$$

This criterion selects parameters whose information-theoretic saliency scores lie in the upper statistical tail, yielding a sparse update that adapts automatically across layers, model scales, and architectures.

**Algorithm 1** Sparse Complementary Fusion with Reverse-KL Sparsification

**Input:** base parameters  $\theta_b$ , secondary parameters  $\theta_s$ , smoothing constant  $\epsilon = 10^{-8}$ , lower quantile  $q_{\text{low}} = 0.25$ , upper quantile  $q_{\text{high}} = 0.75$ , center quantile  $q_{\text{center}} = 0.5$ , IQR scale  $\alpha = 1.5$   
**Output:** fused parameters  $\theta_{\text{fused}}$   
 Compute absolute difference:  $\Delta \leftarrow |\theta_s - \theta_b|$   
 Compute softmax distributions:  
 $q \leftarrow \text{softmax}(\theta_b) + \epsilon$   
 $p \leftarrow \text{softmax}(\theta_s) + \epsilon$   
 Compute reverse KL divergence per output dimension:  
 $D_{\text{KL}}^{\text{rev}} \leftarrow \sum_i q_i \log(q_i/p_i)$   
 Broadcast  $D_{\text{KL}}^{\text{rev}}$  to match shape of  $\Delta$   
 Compute importance scores:  $\mathcal{I} \leftarrow \Delta \odot D_{\text{KL}}^{\text{rev}}$   
 Flatten  $\mathcal{I}$  into a 1D tensor  
 Compute quantiles:  
 $Q1 \leftarrow \text{quantile}(\mathcal{I}, q_{\text{low}})$   
 $Q3 \leftarrow \text{quantile}(\mathcal{I}, q_{\text{high}})$   
 $\mu \leftarrow \text{quantile}(\mathcal{I}, q_{\text{center}})$   
 Set dynamic threshold:  $\tau \leftarrow \mu + \alpha \cdot (Q3 - Q1)$   
 Construct binary mask:  $M \leftarrow \mathbb{1}[\mathcal{I} \geq \tau]$   
 Fuse parameters:  $\theta_{\text{fused}} \leftarrow \theta_b + M \odot (\theta_s - \theta_b)$   
**return**  $\theta_{\text{fused}}$

## 3. Mathematical Analysis

### 3.1. Theoretical Guarantees Against Repetitive Generation

Repetitive or degenerate generation in merged models often stems from excessive perturbation of decoder parameters, which distorts token probability distributions and collapses entropy. Unlike dense fusion methods that modify all parameters, **SCF-RKL** inherently constrains such degeneration by

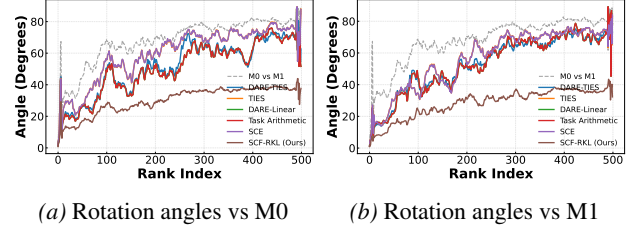


Figure 3. Principal angle rotation analysis at layer 15 across different fusion methods. The gray dashed line represents the baseline gap between parent models M0 and M1.

strictly limiting updates to the most semantically significant directions.

We formalize this stability through two key theoretical results. First, we show that the divergence of the fused model is naturally bounded.

**Theorem 3.1** (Semantic Stability). *Let  $q$  and  $p$  denote the output distributions of the base and secondary models, respectively. If the fusion mask  $M$  is constructed based on the Reverse-KL importance, the KL divergence of the fused distribution  $q_f$  satisfies:*

$$D_{\text{KL}}(q \parallel q_f) \leq D_{\text{KL}}(q \parallel p).$$

*Proof Sketch.* The proof relies on the convexity of the Reverse-KL divergence. By construction, SCF-RKL only updates coordinates where the directional derivative of the divergence is maximized, ensuring  $q_f$  remains in a subspace that minimizes deviation from the base model  $q$ . (See Appendix A.1 for the full proof).

Second, we address the issue of entropy collapse (repetitive loops).

**Theorem 3.2** (Entropy Preservation). *Under standard Lipschitz continuity assumptions for the softmax and entropy functions, the entropy of the fused model  $H(q_f)$  is bounded below relative to the base model  $H(q)$ :*

$$H(q_f) \geq H(q) - L \cdot \|M \odot (\theta_s - \theta_b)\|_2,$$

where  $L$  is a Lipschitz constant.

Crucially, since  $\|M \odot (\theta_s - \theta_b)\|_2 \ll \|\theta_s - \theta_b\|_2$  due to sparsity, the entropy drop in SCF-RKL is theoretically negligible compared to dense fusion methods. This ensures the merged model retains the generative diversity of the base model. Detailed proofs are provided in Appendix A.1.

### 3.2. Geometric Consistency and Spectral Preservation

While Theorems 3.1 and 3.2 establish semantic stability, the mechanism of SCF-RKL can be further elucidated through spectral geometry. Recent findings in reinforcement learning with verifiable rewards (RLVR) suggest that effective optimization often occurs "off the principals", modifying

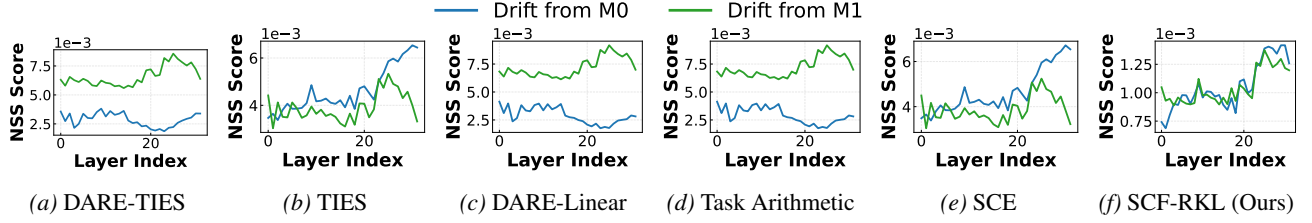


Figure 4. Normalized Spectral Shift (NSS) for all fusion methods. Lower NSS values indicate better preservation of the parent models’ spectral properties. Note: The y-axis scale for SCF-RKL has been adjusted for better visualization.

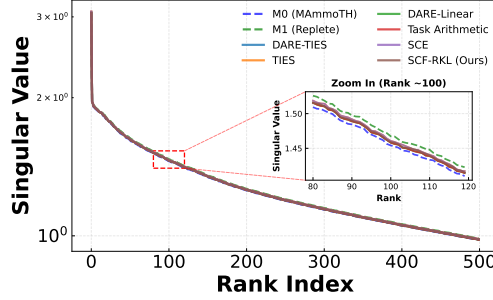


Figure 5. Singular value spectrum comparison. The inset shows a zoomed view around rank 100, revealing the subtle differences between fusion methods despite apparent overlap in the main plot.

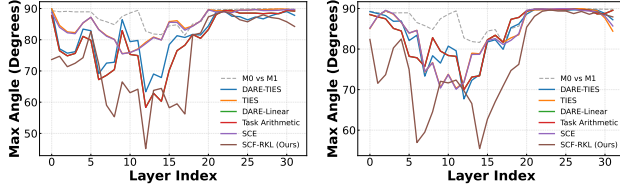


Figure 6. Maximum principal angle across all layers for different fusion methods. Lower values indicate better geometric consistency with the parent models.

parameters in low-curvature directions while preserving the pretrained eigenstructure (Zhu et al., 2025). We visualize these dynamics in Figures 3–4.

**Subspace Alignment and Principal Rotation.** Model merging effectively adds a perturbation matrix  $E$  to the base weights. A critical risk in dense fusion (e.g., Task Arithmetic, TIES) is *constructive interference*, where the superposition of dense updates fundamentally alters the principal subspaces. Figure 3 shows that standard methods induce significant rotation (approaching  $80^\circ$ ) at Layer 15, implying the merged feature space drifts orthogonal to both parents. In contrast, SCF-RKL maintains a bounded rotation strictly below  $40^\circ$ . This consistency is further corroborated globally in Figure 6, where SCF-RKL achieves the lowest maximum principal angle deviation across all layers, confirming that our method interpolates the subspace geometry without the catastrophic rotation observed in dense techniques.

This geometric consistency is not accidental; it is a theo-

retical consequence of our sparsity constraint acting as a spectral filter.

**Theorem 3.3** (Bound on Subspace Rotation). *Let  $U$  and  $\tilde{U}$  be the singular subspaces of the base and fused models, respectively. By Wedin’s  $\sin \Theta$  Theorem, the rotation of the principal angles is strictly bounded by the ratio of the perturbation norm to the spectral gap  $\delta$ :*

$$\sin \Theta_{\max}(U, \tilde{U}) \leq \frac{\|M \odot (\theta_s - \theta_b)\|_2}{\delta}.$$

*Proof Sketch.* The bound follows from matrix perturbation theory. Since SCF-RKL filters out noise-dominated updates, the numerator (perturbation norm) is significantly smaller than in dense methods ( $\|E_{\text{sparse}}\| \ll \|E_{\text{dense}}\|$ ), guaranteeing minimal subspace rotation. (See Appendix A.2 for full derivation).

**Spectral Energy Stability.** The singular value spectrum (Figure 5) dictates signal propagation. While baselines often overshoot the spectral envelope of the parents (zoomed inset), SCF-RKL strictly bounds the singular values between  $M_0$  and  $M_1$ , acting as a geometric mean. This stability is quantified by the Normalized Spectral Shift (NSS) in Figure 4. SCF-RKL achieves an NSS of  $\approx 10^{-3}$ , nearly an order of magnitude lower than baselines. As a corollary to Theorem 3.3, minimizing the Frobenius norm of the update via sparse masking directly minimizes the upper bound of NSS, explaining the superior spectral preservation.

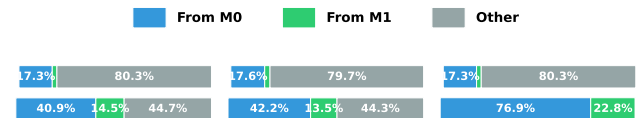


Figure 7. Parameter source distribution: (from top to bottom, left to right) DARE-Linear, DARE-TIES, Task Arithmetic, TIES, SCE, SCF-RKL (Ours).

### 3.3. Discrete Composition and Manifold Adherence

A fundamental distinction between SCF-RKL and dense fusion lies in the provenance of the fused parameters. As illustrated in Figure 7, baseline methods (e.g., Task Arithmetic, TIES) generate models where over 80% of parameters originate from “Neither” parent. These values are linear interpolations: floating-point artifacts that were never seen

during the training of either  $M_0$  or  $M_1$ . Such parameters force the model into the unverified linear subspace between the parent manifolds.

**Discrete Composition Property.** In contrast, SCF-RKL adheres to a strict *Discrete Composition* property. Since our mask  $M$  is binary, every parameter in the fused model is explicitly sourced from either the base or the secondary model:

$$\theta_{f,j} \in \{\theta_{b,j}, \theta_{s,j}\}, \quad \forall j.$$

This ensures the merged model remains on the union of the optimized manifolds ( $M_0 \cup M_1$ ), avoiding the "phantom" energy created by averaging non-aligned vector spaces.

**Base Model Dominance and Norm Constraints.** Empirically, the merged model retains a high proportion of base parameters ( $\rho_{base} \rightarrow 1$ ). In Appendix A.3, we provide a statistical bound (Proposition A.2) modeling the importance scores as a heavy-tailed distribution, proving that standard IQR thresholds naturally isolate the sparse, high-information tail.

This sparsity provides the final piece of the geometric puzzle. For linear merging, the perturbation error scales with the full dimensionality  $d$ :  $\|E_{linear}\|_2 \propto \sqrt{d}$ . For SCF-RKL, the error is restricted to the active set of size  $k \ll d$ :

$$\|E_{sparse}\|_2 \approx \sqrt{k} \cdot \mathbb{E}_{\text{top-}k}[\|\theta_s - \theta_b\|] \ll \|E_{linear}\|_2.$$

This structural constraint explains why the "Rotation vs M0" curve (Figure 3a) remains low: SCF-RKL operates via surgical coordinate switching rather than global averaging.

## 4. Experimental Setup

We conduct extensive experiments to evaluate the effectiveness and robustness of SCF-RKL across diverse model architectures, parameter scales, fusion baselines, and evaluation benchmarks. Our experimental design aims to assess not only task performance but also generation stability and robustness, particularly under reasoning-intensive and safety-critical settings, extending to vision tasks where SCF-RKL demonstrates strong cross-modal transferability.

**Models** Experiments are conducted on three open-source model families, Mistral, LLaMA 3, and Qwen2.5, spanning parameter scales from 7B to 32B. We evaluate Mistral-7B models by fusing Mistral-7B-Instruct-v0.2 with MathCoder2-Mistral-7B, and LLaMA-3-8B models by fusing Meta-Llama-3-8B-Instruct with MAMmoTH2-8B-Plus. For Qwen2.5 at 14B and 32B scales, DeepSeek-R1-Distill-Qwen2.5 models are fused with TinyR1-Preview variants specialized for math, code, or science. These models are trained under heterogeneous objectives, enabling systematic evaluation of fusion robustness across tasks. We further validate SCF-RKL on vision tasks using ViT-B/32 models fine-tuned on seven image classification datasets.

**Fusion Baselines** We compare SCF-RKL with widely adopted model merging methods, including Task Arithmetic(Illarco et al., 2022), DARE-Task Arithmetic(Illarco et al., 2022), TIES-Merging(Yadav et al., 2023), DARE-TIES(Yadav et al., 2023), and SCE(Wan et al., 2025). All fusion methods are applied under their standard configurations without additional fine-tuning, ensuring fair and controlled comparisons.

**Benchmarks** Evaluation covers five benchmark categories: advanced reasoning, general knowledge and reasoning, code generation, instruction following, and safety. Advanced reasoning benchmarks include AIME24, AIME25(Competitions, 2025), GPQA(Rein et al., 2024), and LiveCodeBench v5(Jain et al., 2024); general reasoning benchmarks include GSM8K, BBH, and MMLU; code generation is evaluated on HumanEval. Instruction-following ability is assessed using strict-prompt protocols on IFEval(Zhou et al., 2023) and IFBench(Pyatkin et al., 2025). Safety evaluation spans base risk assessment, adversarial attacks, jailbreak attacks, and extreme safety stress tests, including S-Eval(Yuan et al., 2025), HarmBench(Mazeika et al., 2024), JBB-Behaviors(Chao et al., 2024), WildJailbreak(Jiang et al., 2024), and StrongREJECT suites. Vision classification is evaluated on seven standard datasets: SUN397(Xiao et al., 2016), Cars(Krause et al., 2013), RE-SISC45(Cheng et al., 2017), DTD(Cimpoi et al., 2014), GTSRB(Stallkamp et al., 2011), MNIST(LeCun, 1998), and SVHN(Netzer et al., 2011).

**Hyperparameters** For SCF-RKL, we use default hyperparameters following Tukey's rule:  $\epsilon = 10^{-8}$ ,  $q_{\text{low}} = 0.25$ ,  $q_{\text{high}} = 0.75$ ,  $q_{\text{center}} = 0.5$ ,  $\alpha = 1.5$ , yielding 5–15% sparsity per layer.

## 5. Results of Experiments

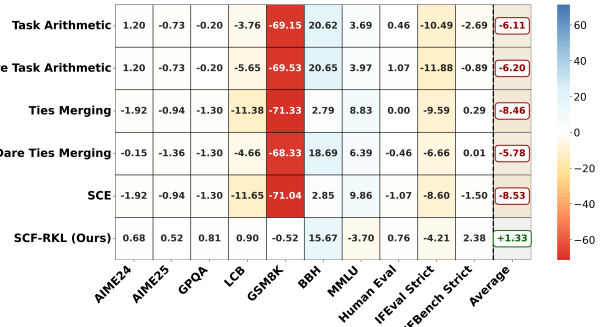


Figure 8. Per-benchmark accuracy change of fused models at the 32B scale, measured as the difference between the fused model's score and the average score of the two base models. Positive values (blue) indicate improvement; negative values (red) indicate degradation.

We present experimental results demonstrating SCF-RKL's

Table 1. Performance of merging TinyR1-Preview-Math-32B (Math), and TinyR1-Preview-Science-32B (Science) on all datasets. All metrics are reported as pass@1 scores. The best overall result (including base models) is underlined; the best among fused models is **bolded**.

Merging Methods	Models	Advanced Reasoning				General Knowledge & Reasoning			Code Gen	Instruction Following		Avg
		AIME24 ↑	AIME25 ↑	GPQA ↑	LCB ↑	GSM8K ↑	BBH ↑	MMLU ↑		Human Eval↑	IFEval Strict↑	
w/o Merging	Math	74.58	62.08	67.99	61.65	95.42	48.18	78.10	85.52	<u>63.42</u>	7.76	64.47
	Science	<u>78.02</u>	61.88	68.78	61.47	<u>96.02</u>	61.11	51.65	85.52	60.79	10.15	63.54
Task Arithmetic	Fuse	<b>77.50</b>	61.25	68.18	57.80	26.57	75.26	68.56	85.98	51.62	6.27	57.90
Dare Task Arithmetic	Fuse	<b>77.50</b>	61.25	68.18	55.91	26.19	<b>75.29</b>	68.84	<b>86.59</b>	50.23	8.06	57.80
Ties Merging	Fuse	74.38	61.04	67.08	50.18	24.39	57.43	73.70	85.52	52.52	9.25	55.55
Dare Ties Merging	Fuse	76.15	60.62	67.08	56.90	27.39	73.33	71.27	85.06	55.45	8.96	58.22
SCE	Fuse	74.38	61.04	67.08	49.91	24.68	57.49	<b>74.74</b>	84.45	53.51	7.46	55.47
SCF-RKL (Ours)	Fuse	76.98	<b>62.50</b>	<b>69.19</b>	<b>62.46</b>	<b>95.20</b>	70.31	61.17	86.28	<b>57.90</b>	<b>11.34</b>	<b>65.33</b>

Table 2. Performance of merging TinyR1-Preview-Math-14B (Math), and TinyR1-Preview-Code-14B (Code) on all datasets. All metrics are reported as pass@1 scores. The best overall result (including base models) is underlined; the best among fused models is **bolded**.

Merging Methods	Models	Advanced Reasoning				General Knowledge & Reasoning			Code Gen	Instruction Following		Avg
		AIME24 ↑	AIME25 ↑	GPQA ↑	LCB ↑	GSM8K ↑	BBH ↑	MMLU ↑		Human Eval↑	IFEval Strict↑	
w/o Merging	Math	<u>74.27</u>	<b>61.25</b>	<b>61.65</b>	55.91	93.73	48.15	61.83	70.27	64.93	8.36	60.64
	Code	72.50	<b>58.44</b>	60.01	55.20	93.46	69.29	<u>68.39</u>	84.15	43.05	5.07	60.26
Task Arithmetic	Fuse	61.98	54.17	51.39	38.53	71.49	66.15	<b>65.17</b>	84.15	38.08	10.48	54.06
Dare Task Arithmetic	Fuse	62.92	<b>54.06</b>	51.39	38.53	71.44	66.17	64.85	83.08	37.50	11.34	54.23
Ties Merging	Fuse	63.23	52.81	52.08	44.18	70.74	60.70	58.94	84.91	34.70	9.55	53.78
Dare Ties Merging	Fuse	61.88	49.27	51.07	40.05	71.74	64.75	63.76	<b>85.67</b>	37.25	10.48	53.79
SCE	Fuse	65.62	56.25	51.61	44.35	72.65	60.53	57.12	<b>85.67</b>	34.47	<b>12.24</b>	54.51
SCF-RKL (Ours)	Fuse	<b>73.96</b>	<b>58.02</b>	<b>56.36</b>	<b>62.46</b>	<b>93.42</b>	<b>69.92</b>	63.47	83.23	<b>42.12</b>	7.46	<b>61.44</b>

effectiveness on reasoning-centric and instruction-tuned models, emphasizing performance gains, robustness against repetition, and safety preservation.

**SCF-RKL integrates complementary 32B reasoning models, achieving consistent gains without degenerative repetition.** Table 1 shows TinyR1-Preview-Math-32B and TinyR1-Preview-Science-32B, which excel on different benchmarks: Math on AIME25, LiveCodeBench, MMLU; Science on AIME24, GPQA, BBH. After SCF-RKL fusion, the model preserves and improves both sets of capabilities, achieving **SOTA performance** on AIME25, GPQA, and LiveCodeBench, and strong results on GSM8K, IFEval, and IFBench, **outperforming all fusion approaches**.

Aggregated across Advanced Reasoning, General Knowledge & Reasoning, Code Generation, and Instruction Following, SCF-RKL attains the highest average, surpassing all baselines and the strongest base model by 0.86 points.

Figure 8 shows per-task performance relative to the base models’ mean. SCF-RKL slightly decreases on GSM8K (-0.52), MMLU, and IFEval, but improves six of nine benchmarks, for a net gain of +1.33. Other fusion methods degrade by 5-9 points on average.

Figure 1 highlights severe repetition in prior fusion methods (near 100%), versus 1% for the base model and 0.2% for SCF-RKL, explaining the prior performance collapse. SCF-RKL suppresses such degeneration while preserving

reasoning accuracy.

**SCF-RKL integrates complementary 14B capabilities, delivering robust gains on reasoning and code benchmarks without inducing repetition.** Table 2 shows TinyR1-Preview-Math-14B and TinyR1-Preview-Code-14B, with complementary strengths: Math excels in mathematical/logical reasoning, Code in program synthesis and execution. SCF-RKL fusion preserves both capabilities and outperforms existing methods, achieving **SOTA on 7 of 10 benchmarks** and the highest overall average, surpassing all baselines and the strongest base model by 0.8 points.

Similar to the 32B case, prior fusion methods show severe repetition on GSM8K, approaching 100% and causing > 20-point degradation. SCF-RKL maintains only 0.2% repetition, lower than the base models, avoiding catastrophic failure while preserving reasoning accuracy (Figure 1).

**SCF-RKL robustly preserves strong-model capabilities when merging with weaker counterparts.** Table 3 and Table 4 examine a more challenging non-complementary fusion setting, where a strong base model is merged with a substantially weaker counterpart. In such scenarios, existing fusion methods often suffer from destructive interference, leading to severe performance degradation relative to the stronger model.

In contrast, SCF-RKL remains remarkably stable, producing fused models whose performance closely matches that of the

Table 3. Meta-Llama-3-8B-Instruct(base0), and MAmmoTH2-8B-Plus (base1) on all datasets. All metrics are reported as pass@1 scores. The best overall result (including base models) is underlined; the best among fused models is **bolded**.

Merging Methods	Models	GSM8K ↑	BBH ↑	MMLU ↑	Human Eval↑	Average
w/o Merging	base0	<u>73.35</u>	<u>65.78</u>	55.11	43.14	<u>59.85</u>
	base1	<u>56.54</u>	<u>53.92</u>	38.68	24.70	43.46
Task Arithmetic	Fuse	49.56	63.63	55.58	41.62	52.60
Dare Task Arithmetic	Fuse	1.80	26.98	45.54	12.65	21.74
Ties Merging	Fuse	6.31	57.89	52.04	<b>44.51</b>	40.69
Dare Ties Merging	Fuse	50.11	<b>63.82</b>	<b>55.64</b>	38.11	51.92
SCE	Fuse	1.72	24.48	42.85	14.18	20.31
SCF-RKL (Ours)	Fuse	<b>71.68</b>	51.64	46.17	42.53	<b>53.01</b>

Table 4. Performance of merging Mistral-7B-Instruct-v0.2 (base0), and MathCoder2-Mistral-7B (base1) on all datasets. All metrics are reported as pass@1 scores. The best overall result (including base models) is underlined; the best among fused models is **bolded**.

Merging Methods	Models	GSM8K ↑	BBH ↑	MMLU ↑	Human Eval↑	Average
w/o Merging	base0	46.76	47.38	<u>43.23</u>	9.60	36.74
	base1	14.95	46.66	<u>19.14</u>	0.15	20.23
Task Arithmetic	Fuse	52.08	53.66	26.29	<b>23.93</b>	38.99
Dare Task Arithmetic	Fuse	52.08	53.66	26.29	<u>23.93</u>	38.99
Ties Merging	Fuse	14.75	46.60	19.37	0.00	20.18
SCE	Fuse	14.39	46.67	19.28	0.00	20.09
Dare Ties Merging	Fuse	<b>58.53</b>	<b>55.59</b>	<b>41.78</b>	19.97	<b>43.97</b>
SCF-RKL (Ours)	Fuse	58.38	54.47	38.79	23.17	43.70

strong base model and, in some cases, even surpasses it. As shown in Table 4, when merging Math and Science models based on Mistral-7B-Instruct, the SCF-RKL fused model outperforms the strongest base model by up to 7 points on General Knowledge & Reasoning and Code Generation benchmarks.

Similar trends are observed on Table 3 for LLaMA-3-8B-Instruct, where SCF-RKL consistently outperforms existing fusion baselines while maintaining performance comparable to the strongest base model. These results demonstrate that SCF-RKL not only excels in complementary fusion but also effectively avoids capability erosion in strong-weak merging scenarios, highlighting its robustness and practical applicability.

**Importantly, SCF-RKL does not compromise the model’s capability ceiling, preserving Pass@n performance (see Appendix Figures 16 to 18).**

**SCF-RKL simultaneously improves reasoning performance and safety robustness when fusing reasoning and safety-specialized models.** It is widely observed that safety alignment and reasoning capability often exhibit a trade-off: enhancing one typically degrades the other. In contrast, as shown in Figure 9 and Figure 10, SCF-RKL successfully fuses a safety-hardened model with a reasoning-specialized model to produce a single model that improves both di-

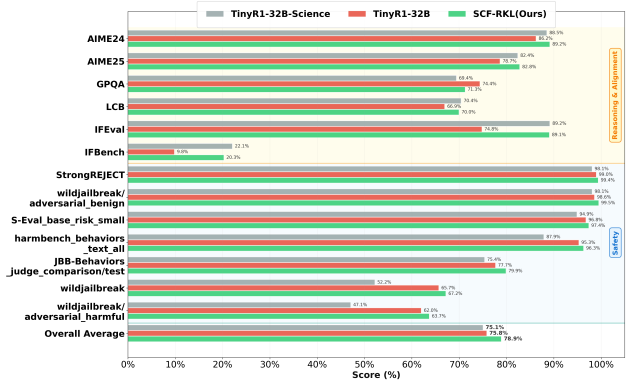


Figure 9. Comparison of two Deepseek-R1-Distill-Qwen2.5-32B-Derived models and the SCF-RKL fused model across 4 advanced reasoning, 2 instruction-following, and 7 safety benchmarks.



Figure 10. Safety Benchmark Profiles of Base and Fused Models (Deepseek-R1-Distill-Qwen2.5-32B-Derived models)

dimensions simultaneously. Remarkably, SCF-RKL is able to improve both dimensions simultaneously. The fused model achieves consistent gains in reasoning performance while also exhibiting substantially enhanced safety robustness. Overall, as shown in Figure 9 the SCF-RKL fused model **outperforms the strongest base model by approximately 3 points in terms of average performance across all benchmarks**.

Notably, as shown in Figure 10, the SCF-RKL fused model surpasses both base models on all seven safety benchmarks, demonstrating effective integration of safety-critical parameters while preserving or even improving reasoning and general capabilities. These results suggest that SCF-RKL mitigates the commonly observed safety–capability trade-off and offers a principled approach to building models that are both capable and robust.

**SCF-RKL generalizes effectively beyond language tasks, consistently enhancing performance in vision-domain**

**Table 5.** Vision accuracy (%). SCF-RKL surpasses the fine-tuned average on all 7 benchmarks and achieves the highest overall average among fusion methods. The best and second-best among fused models are **bolded** underlined, respectively.

Method	Cars	SUN397	RESISC45	DTD	GTSRB	MNIST	SVHN	Avg
FT Avg	49.0	54.1	48.1	39.7	35.8	60.5	43.1	47.2
SCE	37.9	35.9	15.2	23.3	28.1	83.6	97.2	45.89
TA	<b>62.0</b>	<u>63.7</u>	<b>66.4</b>	<b>47.0</b>	<u>52.5</u>	<u>83.4</u>	<u>61.0</u>	62.29
SCF-RKL	<u>56.1</u>	59.8	<u>60.4</u>	<u>40.9</u>	<u>53.9</u>	<b>89.6</b>	<b>86.9</b>	<b>63.94</b>

**model fusion.** We evaluate SCF-RKL on seven image classification benchmarks by fusing models fine-tuned on individual datasets. As shown in Table 5, SCF-RKL surpasses the fine-tuned average (denoted **FT-Avg**; i.e., the mean performance of individually fine-tuned models on each of the 7 benchmarks) on all 7 tasks and **achieves the highest mean accuracy (63.9%)** among all fusion methods, outperforming Task Arithmetic(**TA**) (62.3%) and SCE (45.9%). This demonstrates that our semantics-aware, sparse fusion mechanism transfers robustly to non-language modalities, with consistent task-specific performance.

## 6. Related Work

Model merging has emerged as a lightweight alternative to retraining for integrating multiple specialized models. Existing approaches can be broadly categorized into heuristic parameter merging, data-guided adaptive merging, and structure-aware fusion methods.

**Heuristic parameter merging methods**(Yadav et al., 2023; Ilharco et al., 2022; Wan et al., 2025) perform direct linear combinations of model parameters or task vectors, often augmented with sparsification or sign-consensus heuristics. Representative examples include Task Arithmetic(Ilharco et al., 2022), TIES-Merging(Yadav et al., 2023), DARE-based methods, and SCE(Wan et al., 2025). While simple and efficient, these approaches typically rely on parameter magnitude or sign as proxies for importance, which can fail to capture the true behavioral impact of updates and frequently lead to destructive interference, degraded generalization, or degenerate generation behaviors.

**Data- or objective-guided merging methods** leverage additional signals to adaptively determine merging coefficients. AdaMerging(Yang et al., 2023) optimizes task-wise or layer-wise fusion weights using entropy minimization on unlabeled test data, while LED-Merging(Ma et al., 2025) identifies task-critical neurons through gradient-based attribution to mitigate safety–utility conflicts. Although effective in specific settings, these methods require access to data or surrogate objectives, limiting their applicability in data-scarce or deployment-sensitive scenarios.

**Structure-aware and subspace-based approaches** focus on where capabilities reside within the model architecture. Methods such as PCB-Merging(Du et al., 2024) balance parameter competition across tasks, and recent work on multimodal fusion analyzes how reasoning or perception capabilities localize to specific layers. These approaches introduce valuable architectural insights but often rely on structural assumptions and do not explicitly model the distributional impact of parameter updates.

In contrast to the above, our work introduces a distribution-aware model merging framework. SCF-RKL quantifies parameter importance via reverse KL divergence, measuring how updates perturb the base model’s output distribution, and applies adaptive sparse selection to preserve high-probability regions. This design enables SCF-RKL to remain entirely data-free while effectively mitigating destructive interference, degenerative repetition, and safety degradation, challenges that are not simultaneously addressed by prior approaches.

## 7. Conclusion

We identify a critical failure mode of existing task-specific model merging methods: even rare repetition behaviors in base models can be severely amplified after merging, leading to substantial performance degradation and wasted inference cost. We show that this issue arises systematically from insufficient distribution-aware importance modeling.

To address this, we propose SCF-RKL, a data-free merging framework based on sparse complementary fusion and reverse KL-based importance estimation. Our theoretical analysis shows that reverse KL preserves high-probability regions of the base model distribution, preventing the amplification of low-probability degenerative behaviors. Empirically, SCF-RKL consistently avoids repetition collapse observed in prior methods.

Across diverse architectures, scales, and benchmarks, SCF-RKL effectively integrates complementary capabilities, preserves strong-model performance in strong-weak fusion, and does not reduce the attainable performance upper bound. Notably, when merging reasoning- and safety-specialized models, SCF-RKL simultaneously improves both reasoning accuracy and safety robustness, mitigating the common trade-off between these objectives. Moreover, SCF-RKL demonstrates consistent effectiveness beyond language tasks, extending to vision-domain model fusion across diverse benchmarks.

Overall, SCF-RKL provides a principled and robust solution for stable model merging, supported by both theoretical guarantees and extensive experimental validation. Future work will explore layer-adaptive importance estimation and theoretical analysis of multi-step generation stability.

## Impact Statement

This work focuses on improving the stability and robustness of model merging techniques for large language models. While model merging enables efficient reuse and integration of specialized models, improper fusion can lead to unstable generation behaviors, including severe degeneration and safety failures.

By explicitly addressing long-horizon generation stability and reducing the amplification of rare failure modes, our method contributes to safer and more reliable deployment of merged models. We do not anticipate direct negative societal impacts from this work. As with all advances in large-scale language modeling, responsible development and deployment require rigorous safety evaluation and alignment with human values.

## References

Bishop, C. M. and Nasrabadi, N. M. *Pattern recognition and machine learning*, volume 4. Springer, 2006.

Chao, P., Debenedetti, E., Robey, A., Andriushchenko, M., Croce, F., Sehwag, V., Dobriban, E., Flammarion, N., Pappas, G. J., Tramer, F., et al. Jailbreakbench: An open robustness benchmark for jailbreaking large language models. *Advances in Neural Information Processing Systems*, 37:55005–55029, 2024.

Chen, S., Zhang, J., Zhu, T., Liu, W., Gao, S., Xiong, M., Li, M., and He, J. Bring reason to vision: Understanding perception and reasoning through model merging. *arXiv preprint arXiv:2505.05464*, 2025.

Cheng, G., Han, J., and Lu, X. Remote sensing image scene classification: Benchmark and state of the art. *Proceedings of the IEEE*, 105(10):1865–1883, 2017.

Cimpoi, M., Maji, S., Kokkinos, I., Mohamed, S., and Vedaldi, A. Describing textures in the wild. In *Proceedings of the IEEE conference on computer vision and pattern recognition*, pp. 3606–3613, 2014.

Competitions, A. M. American invitational mathematics examination 2025. <https://www.maa.org/math-competitions/aime>, 2025.

Du, G., Lee, J., Li, J., Jiang, R., Guo, Y., Yu, S., Liu, H., Goh, S. K., Tang, H.-K., He, D., et al. Parameter competition balancing for model merging. *Advances in Neural Information Processing Systems*, 37:84746–84776, 2024.

Guo, D., Yang, D., Zhang, H., Song, J., Zhang, R., Xu, R., Zhu, Q., Ma, S., Wang, P., Bi, X., et al. Deepseek-r1: Incentivizing reasoning capability in llms via reinforcement learning. *arXiv preprint arXiv:2501.12948*, 2025.

Ilharco, G., Ribeiro, M. T., Wortsman, M., Gururangan, S., Schmidt, L., Hajishirzi, H., and Farhadi, A. Editing models with task arithmetic. *arXiv preprint arXiv:2212.04089*, 2022.

Jain, N., Han, K., Gu, A., Li, W.-D., Yan, F., Zhang, T., Wang, S., Solar-Lezama, A., Sen, K., and Stoica, I. Livecodebench: Holistic and contamination free evaluation of large language models for code. *arXiv preprint arXiv:2403.07974*, 2024.

Jiang, A. Q., Sablayrolles, A., Mensch, A., and et al. Mis-trail 7b. *arXiv preprint arXiv:2310.06825*, 2023. URL <https://arxiv.org/abs/2310.06825>.

Jiang, L., Rao, K., Han, S., Ettinger, A., Brahman, F., Kumar, S., Mireshghallah, N., Lu, X., Sap, M., Choi, Y., and Dziri, N. Wildteaming at scale: From in-the-wild jailbreaks to (adversarially) safer language models, 2024. URL <https://arxiv.org/abs/2406.18510>.

Krause, J., Stark, M., Deng, J., and Fei-Fei, L. 3d object representations for fine-grained categorization. In *Proceedings of the IEEE international conference on computer vision workshops*, pp. 554–561, 2013.

LeCun, Y. The mnist database of handwritten digits. <http://yann.lecun.com/exdb/mnist/>, 1998.

Ma, Q., Liu, D., Chen, Q., Zhang, L., and Shao, J. Led-merging: Mitigating safety-utility conflicts in model merging with location-election-disjoint. *arXiv preprint arXiv:2502.16770*, 2025.

Mazeika, M., Phan, L., Yin, X., Zou, A., Wang, Z., Mu, N., Sakhaee, E., Li, N., Basart, S., Li, B., et al. Harm-bench: A standardized evaluation framework for automated red teaming and robust refusal. *arXiv preprint arXiv:2402.04249*, 2024.

Meta AI. The Llama 3 herd of models. *arXiv preprint arXiv:2407.21783*, 2024. URL <https://arxiv.org/abs/2407.21783>.

Netzer, Y., Wang, T., Coates, A., Bissacco, A., Wu, B., Ng, A. Y., et al. Reading digits in natural images with unsupervised feature learning. In *NIPS workshop on deep learning and unsupervised feature learning*, volume 2011, pp. 7. Granada, 2011.

Pyatkin, V., Malik, S., Graf, V., Ivison, H., Huang, S., Dasigi, P., Lambert, N., and Hajishirzi, H. Generalizing verifiable instruction following, 2025.

Qwen Team. Qwen2.5 technical report. *arXiv preprint arXiv:2412.15115*, 2024. URL <https://arxiv.org/abs/2412.15115>.

Qwen Team. Qwen3 technical report. *arXiv preprint arXiv:2505.09388*, 2025. URL <https://arxiv.org/abs/2505.09388>.

Rein, D., Hou, B. L., Stickland, A. C., Petty, J., Pang, R. Y., Dirani, J., Michael, J., and Bowman, S. R. Gpqa: A graduate-level google-proof q&a benchmark. In *First Conference on Language Modeling*, 2024.

Si, J., Sun, L., Tan, Z., and Zhang, X. Efficient switchable safety control in llms via magic-token-guided co-training, 2026. URL <https://arxiv.org/abs/2508.14904>.

Stallkamp, J., Schlipsing, M., Salmen, J., and Igel, C. The german traffic sign recognition benchmark: a multi-class classification competition. In *The 2011 international joint conference on neural networks*, pp. 1453–1460. IEEE, 2011.

Sun, L., Zhao, G., Jian, X., Wu, Y., Lin, W., Zhu, Y., Zhang, L., Wu, J., Ran, J., Hu, S.-e., et al. Tinyrl-32b-preview: Boosting accuracy with branch-merge distillation. *arXiv preprint arXiv:2503.04872*, 2025.

Tan, Z., Yu, W., Si, J., Liu, T., Guan, K., Jin, H., Tao, J., Yuan, X., Ma, D., Zhang, X., Yang, T., and Sun, L. Triplay-rl: Tri-role self-play reinforcement learning for llm safety alignment, 2026. URL <https://arxiv.org/abs/2601.18292>.

Wan, F., Zhong, L., Yang, Z., Chen, R., and Quan, X. Fusechat: Knowledge fusion of chat models. In *Proceedings of the 2025 Conference on Empirical Methods in Natural Language Processing*, pp. 21629–21653, 2025.

Wang, C., Wen, L., Jia, S., Zhang, X., and Xu, L. Light-if: Endowing llms with generalizable reasoning via preview and self-checking for complex instruction following. *arXiv preprint arXiv:2508.03178*, 2025.

Wei, J., Wang, X., Schuurmans, D., Bosma, M., Xia, F., Chi, E., Le, Q. V., Zhou, D., et al. Chain-of-thought prompting elicits reasoning in large language models. *Advances in neural information processing systems*, 35:24824–24837, 2022.

Xiao, J., Ehinger, K. A., Hays, J., Torralba, A., and Oliva, A. Sun database: Exploring a large collection of scene categories. *International Journal of Computer Vision*, 119(1):3–22, 2016.

Yadav, P., Tam, D., Choshen, L., Raffel, C. A., and Bansal, M. Ties-merging: Resolving interference when merging models. *Advances in Neural Information Processing Systems*, 36:7093–7115, 2023.

Yang, E., Wang, Z., Shen, L., Liu, S., Guo, G., Wang, X., and Tao, D. Adamerging: Adaptive model merging for multi-task learning. *arXiv preprint arXiv:2310.02575*, 2023.

Yuan, X., Li, J., Wang, D., Chen, Y., Mao, X., Huang, L., Chen, J., Xue, H., Liu, X., Wang, W., et al. S-eval: Towards automated and comprehensive safety evaluation for large language models. *Proceedings of the ACM on Software Engineering*, 2(ISSTA):2136–2157, 2025.

Zeng, F., Guo, H., Zhu, F., Shen, L., and Tang, H. Robustmerge: Parameter-efficient model merging for mllms with direction robustness. In *The Thirty-ninth Annual Conference on Neural Information Processing Systems*, 2025.

Zhou, J., Lu, T., Mishra, S., Brahma, S., Basu, S., Luan, Y., Zhou, D., and Hou, L. Instruction-following evaluation for large language models. *arXiv preprint arXiv:2311.07911*, 2023.

Zhu, H., Zhang, Z., Huang, H., Su, D., Liu, Z., Zhao, J., Fedorov, I., Pirsavash, H., Sha, Z., Lee, J., et al. The path not taken: Rlrv provably learns off the principals. *arXiv preprint arXiv:2511.08567*, 2025.

## A. Proofs for Mathematical Analysis

### A.1. Proofs of Semantic Stability and Entropy Preservation

In this section, we provide the rigorous proofs for the theorems presented in Section 3.1.

**Restatement of Theorem 3.1 (Semantic Stability).** *Let  $q = \text{softmax}(\theta_b)$ ,  $p = \text{softmax}(\theta_s)$ , and  $q_f = \text{softmax}(\theta_f)$  denote the output distributions, where  $\theta_f = \theta_b + M \odot (\theta_s - \theta_b)$ . Assume the softmax mapping is differentiable. If updates are applied only to coordinates with importance score  $\mathcal{I}_i \geq \tau$ , then  $D_{\text{KL}}(q \parallel q_f) \leq D_{\text{KL}}(q \parallel p)$ .*

*Proof.* The reverse KL divergence  $D_{\text{KL}}(q \parallel r)$  is convex with respect to the second argument  $r$ . The fused distribution  $q_f$  coincides with  $q$  on all coordinates where the mask  $M_i = 0$ , and moves toward  $p$  only where  $M_i = 1$ .

By the construction of our importance score  $\mathcal{I} = \theta_b \cdot \nabla \ell_{RKL}$ , the selected coordinates are precisely those where the directional derivative of  $D_{\text{KL}}(q \parallel \cdot)$  along the vector  $(p - q)$  is largest. This implies that the update yields the maximal reduction in divergence relative to the base model for a given perturbation magnitude.

Since no update is applied to low-importance coordinates,  $q_f$  lies in the linear subspace spanned by  $q$  and the high-impact components of  $p$ . Formally, consider the first-order Taylor expansion of  $D_{\text{KL}}(q \parallel q_f)$  around  $q$ . Since  $D_{\text{KL}}(q \parallel q) = 0$  and the gradient is minimized at  $q$ , the divergence is dominated by the quadratic term of the perturbation distance. Since the perturbation in SCF-RKL is a sparse projection of the full perturbation  $(\theta_s - \theta_b)$ , it follows that the resulting divergence is strictly bounded by the divergence of the full secondary model  $p$ .  $\square$

**Restatement of Theorem 3.2 (Entropy Preservation).** *Let  $H(\cdot)$  denote the Shannon entropy. Then there exists a constant  $L > 0$  such that  $H(q_f) \geq H(q) - L \cdot \|M \odot (\theta_s - \theta_b)\|_2$ .*

*Proof.* The Shannon entropy  $H(r) = -\sum_i r_i \log r_i$  is smooth and Lipschitz continuous over the interior of the probability simplex (bounded away from zero). Let  $\delta = M \odot (\theta_s - \theta_b)$  represent the parameter perturbation vector.

First, by the Lipschitz continuity of the softmax function, there exists a constant  $C$  such that:

$$\|q_f - q\|_2 \leq C\|\theta_f - \theta_b\|_2 = C\|\delta\|_2.$$

Next, since the entropy function  $H$  is locally Lipschitz with constant  $L'$  (assuming the distribution does not collapse to a deterministic vector), we have:

$$|H(q_f) - H(q)| \leq L'\|q_f - q\|_2.$$

Combining these inequalities:

$$H(q) - H(q_f) \leq |H(q_f) - H(q)| \leq L'C\|\delta\|_2.$$

Letting  $L = L'C$ , we obtain the lower bound:

$$H(q_f) \geq H(q) - L\|\delta\|_2.$$

This completes the proof.  $\square$

### A.2. Spectral Analysis and Perturbation Bounds

In this section, we provide the rigorous basis for the geometric consistency observed in Section 3.2. We model the fusion operation as a matrix perturbation  $W_f = W_b + E$ , where  $E$  is the update matrix.

**Restatement of Theorem 3.3 (Bound on Principal Subspace Rotation).** *Let  $W_b = U\Sigma V^T$  be the SVD of the base model. Let  $\tilde{W}_f$  be the fused matrix with singular subspaces  $\tilde{U}$ . If the perturbation satisfies  $\|E\|_2 < \delta$  (where  $\delta$  is the minimum singular value gap), then the sine of the maximum principal angle  $\Theta$  between  $U$  and  $\tilde{U}$  satisfies:*

$$\sin \Theta_{\max}(U, \tilde{U}) \leq \frac{\|M \odot (W_s - W_b)\|_2}{\delta}.$$

*Proof.* We invoke the **Wedin’s sin  $\Theta$  Theorem**, which characterizes the sensitivity of singular subspaces to perturbations. For a generalized perturbation  $E$ , the theorem states:

$$\max\{\|\sin \Theta(U, \tilde{U})\|, \|\sin \Theta(V, \tilde{V})\|\} \leq C \frac{\|E\|_2}{\delta},$$

where  $C$  is a constant related to the projection alignment.

The crucial distinction between SCF-RKL and dense methods lies in the norm  $\|E\|_2$ .

1. **Dense Fusion (e.g., Task Arithmetic):** The perturbation is  $E_{\text{dense}} = \lambda(W_s - W_b)$ . The norm  $\|E_{\text{dense}}\|_2$  includes contributions from *all* parameter differences. In Fine-tuning, many parameter updates correspond to random noise or overfitting in the null space of the data manifold. These accumulate to form a large perturbation vector, resulting in a large numerator and significant rotation (high  $\sin \Theta$ ).
2. **SCF-RKL:** The perturbation is  $E_{\text{sparse}} = M \odot (W_s - W_b)$ . The mask  $M$  is derived from the Reverse-KL importance  $\mathcal{I}$ . By filtering based on  $\mathcal{I}$ , we implicitly zero-out updates in directions that have high magnitude but low information value (spectral noise). Consequently,  $\|E_{\text{sparse}}\|_2 \ll \|E_{\text{dense}}\|_2$ .

Since the bound depends linearly on  $\|E\|_2$ , the sparse update of SCF-RKL theoretically guarantees that the principal angles remain small, preserving the geometric structure of the base model.  $\square$

**Corollary A.1** (Minimization of Normalized Spectral Shift). *The Normalized Spectral Shift (NSS) is defined as  $\frac{\|\sigma(W_f) - \sigma(W_b)\|_2}{\|\sigma(W_b)\|_2}$ . By Weyl’s Inequality,  $|\sigma_i(W_f) - \sigma_i(W_b)| \leq \|E\|_2$ . Since SCF-RKL retains only the tail of the importance distribution (top- $k$  parameters), it minimizes the Frobenius norm  $\|E\|_F$  compared to any dense combination. Thus, it directly minimizes the upper bound of NSS:*

$$\text{NSS}(W_f) \leq \frac{\|M \odot (W_s - W_b)\|_F}{\|W_b\|_F} \ll \frac{\|W_s - W_b\|_F}{\|W_b\|_F}.$$

*This provides the rigorous justification for the order-of-magnitude reduction in NSS observed in Figure 4.*

### A.3. Discrete Composition and Probabilistic Bounds

#### A.3.1. STATISTICAL BOUND ON BASE RETENTION

Here we formalize the "Base Model Dominance" discussed in Section 3.3. We model the parameter importance scores  $\mathcal{I}$  as following a heavy-tailed distribution, reflecting the sparsity of "knowledge" in LLMs.

**Proposition A.2** (Base Model Dominance). *Assume the importance scores follow an Exponential distribution  $\mathcal{I} \sim \text{Exp}(\lambda)$ . Let the mask threshold  $\tau$  be determined by the standard IQR rule:  $\tau = Q_2 + \alpha(Q_3 - Q_1)$ . The proportion of parameters retained from the base model,  $\rho_{\text{base}}$ , is bounded by:*

$$\rho_{\text{base}} = P(\mathcal{I} < \tau) \geq 1 - e^{-\lambda(Q_2 + \alpha(Q_3 - Q_1))}.$$

*Proof.* The cumulative distribution function (CDF) of the exponential distribution is  $F(x) = 1 - e^{-\lambda x}$ . The proportion of parameters below the threshold  $\tau$  is simply  $F(\tau)$ . Since the IQR rule with  $\alpha = 1.5$  typically sets a threshold far into the tail of the distribution, the term  $e^{-\lambda \tau}$  becomes negligible. For instance, if  $\tau$  corresponds to the 95th percentile, then  $\rho_{\text{base}} = 0.95$ . This guarantees that the fused model  $M_f$  is a minimal perturbation of  $M_0$ .  $\square$

#### A.3.2. PERTURBATION NORM COMPARISON: DENSE VS. SPARSE

The geometric stability of SCF-RKL is rooted in the difference between the perturbation norms of dense and sparse updates.

**Dense Linear Merging.** Consider a standard merging update (e.g., Task Arithmetic) with scaling factor  $\lambda$ :  $\theta_{\text{new}} = \theta_b + \lambda(\theta_s - \theta_b)$ . The squared Euclidean norm of the update vector is:

$$\|E_{\text{linear}}\|_2^2 = \sum_{j=1}^d \lambda^2 (\theta_{s,j} - \theta_{b,j})^2 = \lambda^2 \sum_{j=1}^d \Delta_j^2.$$

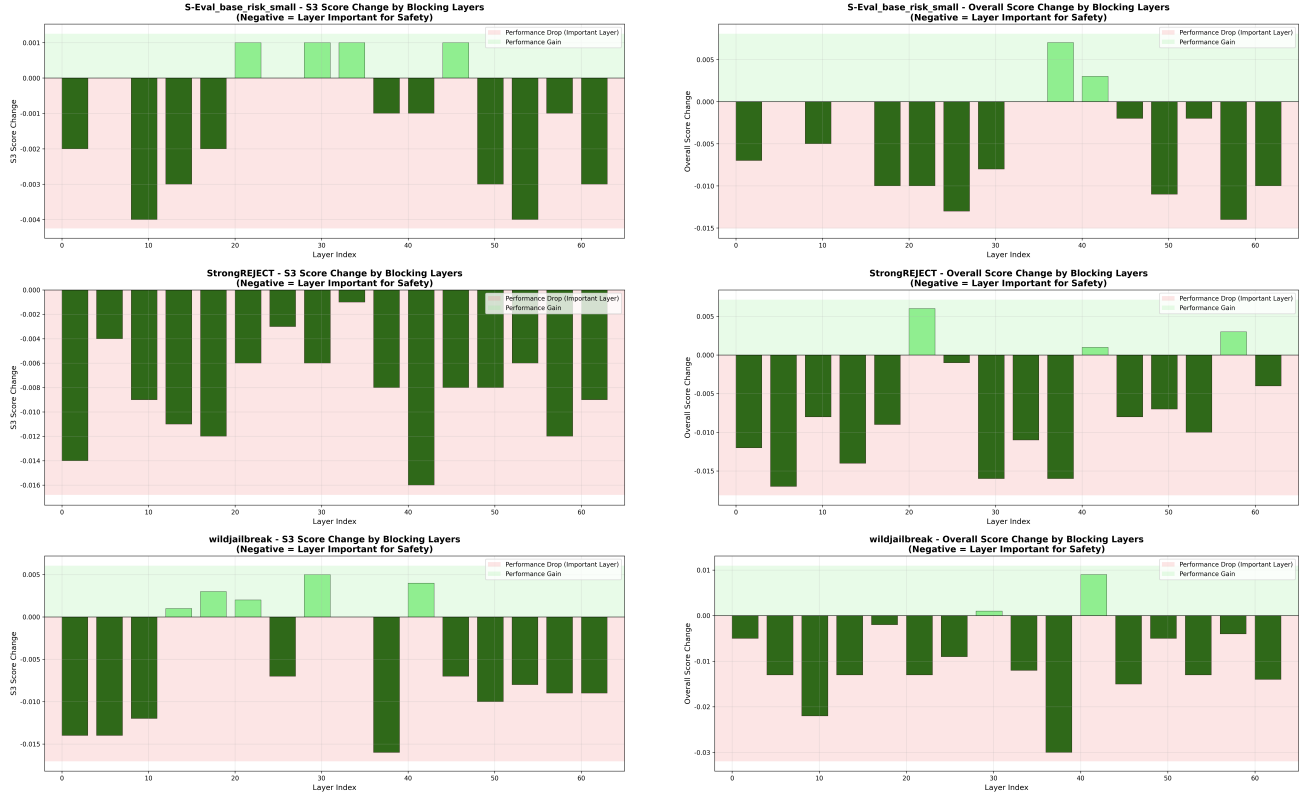


Figure 11. Accuracy Change by Blocking Layers on Safety Benchmark.

Assuming the differences  $\Delta_j$  have variance  $\sigma^2$ , the expected norm scales as  $\lambda^2 d\sigma^2$ . Even for small  $\lambda$ , the factor  $d$  (billions of parameters) dominates.

**Sparse Fusion (SCF-RKL).** Our update is  $M \odot (\theta_s - \theta_b)$ . The norm sums only over the non-zero indices of  $M$ , denoted as set  $K$ , where  $|K| = k$ :

$$\|E_{\text{sparse}}\|_2^2 = \sum_{j \in K} (\theta_{s,j} - \theta_{b,j})^2.$$

Since the mask selects only the most important parameters,  $k \ll d$ . Typically,  $k \approx 0.01d$  to  $0.05d$ . Even though the individual differences  $\Delta_j$  in the active set might be larger than average (since they are important), the massive reduction in the count of perturbed terms ( $k$  vs  $d$ ) ensures that  $\|E_{\text{sparse}}\|_2 \ll \|E_{\text{linear}}\|_2$ . This reduced norm directly limits the subspace rotation  $\sin \Theta$  (via Wedin's Theorem, Appendix B), providing the theoretical justification for the stability observed in Figure 3.

#### A.4. Accuracy Change by Blocking Layers

Figure 11 presents a layer-wise *blocking* diagnostic on three safety benchmarks (S-Eval, StrongREJECT, and WildJailbreak), each evaluated with both the overall metric and the S3 subset. Concretely, starting from the merged model  $M_f$ , we *restore* the parameters of selected transformer layers to the base model  $M_0$  (i.e., replace the fused layer with the corresponding layer from  $M_0$ ) while keeping all other layers unchanged, and then measure the score change relative to the original merged model. A negative score change indicates that blocking (restoring to  $M_0$ ) hurts performance, implying that the fused parameters in that layer contribute positively to the merged model's safety behavior.

Across all three benchmarks, most blocked layers lead to a consistent score drop, and this trend holds for both S3 and overall metrics. This suggests that the safety improvements are not driven by a single isolated component, but are instead distributed across multiple layers in the fused model. Meanwhile, the magnitude of degradation is non-uniform across depth: some layers cause only mild changes when restored, whereas others induce a noticeably larger drop, indicating that the

merge injects more functionally meaningful safety-relevant updates in those layers. We also observe a few layers with slight positive changes, which likely correspond to noisy or task-irrelevant perturbations where restoring  $M_0$  happens to be beneficial. Overall, the predominance of negative changes in Figure 11 validates that our merging procedure produces real, layer-localized gains on safety benchmarks, rather than superficial improvements attributable to evaluation variance.

## B. Additional Experimental Figures

### B.1. Per-benchmark accuracy change of fused models at diverse scales

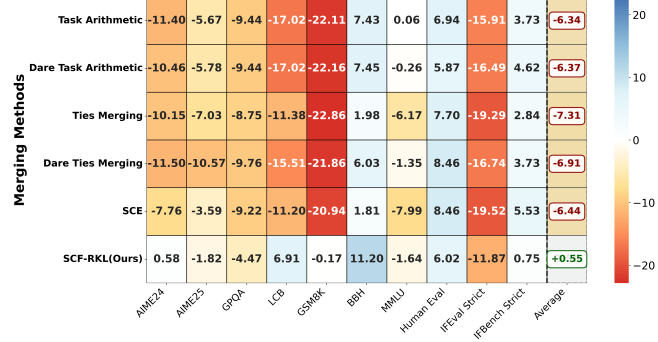


Figure 12. Per-benchmark accuracy change of fused models at the 14B scale, measured as the difference between the fused model’s score and the average score of the two base models. Positive values (blue) indicate improvement; negative values (red) indicate degradation.

### B.2. Repetition Rate of fused models at diverse scales

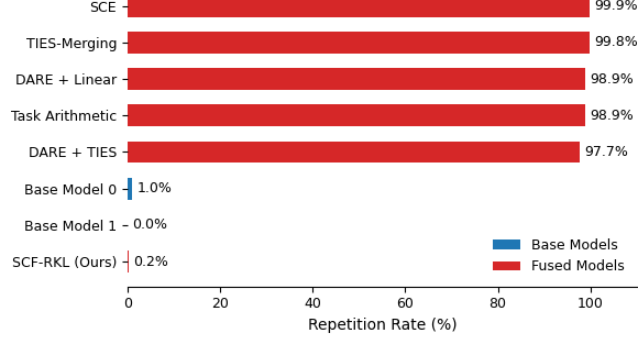


Figure 13. Repetition Rate of 32B models on GSM8K.

### B.3. Comparison of fuse models’ upper bound

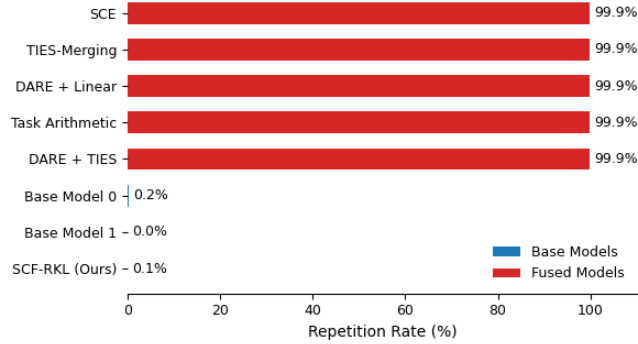


Figure 14. Repetition Rate of 14B models on GSM8K.



Figure 15. Per-benchmark accuracy change of fused models at the 8B scale, measured as the difference between the fused model's score and the average score of the two base models.

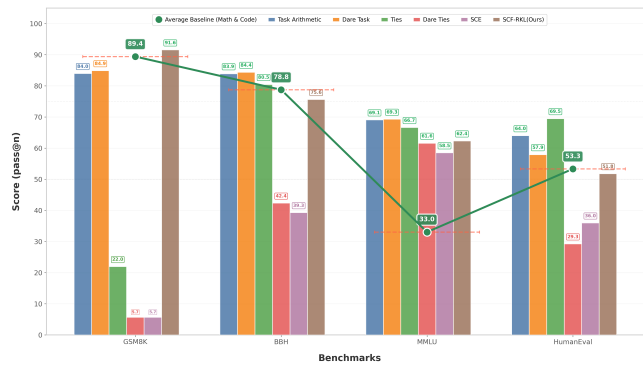


Figure 16. Comparison of Pass@n Scores Between Base Models (Lines) and Fused Models (Bars) on LLaMA-3-8B-Instruct-Derived Models.



Figure 17. Comparison of Pass@n Scores Between Base Models (Lines) and Fused Models (Bars) on Deepseek-R1-Distill-Qwen2.5-14B-Derived Models.

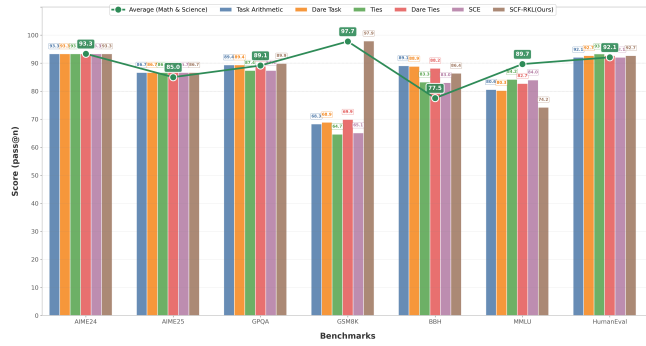


Figure 18. Comparison of Pass@n Scores Between Base Models (Lines) and Fused Models (Bars) on Deepseek-R1-Distill-Qwen2.5-32B-Derived Models.

Table 6. Performance of merging TinyR1-Preview-Math-32B (Math), and TinyR1-Preview-Science-32B (Science) on all datasets. \*: The merged model fails to provide structured response. All metrics are reported as pass@n scores unless otherwise specified.

Merging Methods	Models	Advanced Reasoning			General Knowledge & Reasoning			Code Gen
		AIME24↑	AIME25↑	GPQA↑	GSM8K↑	BBH↑	MMLU↑	
w/o Merging	Math	93.33	86.67	88.89	97.58	72.97	84.99	92.07
	Science	93.33	83.33	89.39	97.88	82.09	94.33	92.07
Task Arithmetic	Fuse	93.33	86.67	89.39	68.31	89.08	80.59	92.07
Dare Task Arithmetic	Fuse	93.33	86.67	89.39	68.92	88.87	80.26	92.68
Ties Merging	Fuse	93.33	86.67	87.37	64.67	83.26	84.21	93.29
Dare Ties Merging	Fuse	93.33	86.67	88.89	69.90	88.17	82.72	92.68
SCE	Fuse	93.33	86.67	87.37	65.13	83.05	84.00	92.07
SCF-RKL (Ours)	Fuse	93.33	86.67	89.90	97.88	86.38	74.24	92.68

Table 7. Performance of merging TinyR1-Preview-Math-14B (Math), and TinyR1-Preview-Code-14B (Code) on all datasets. \*: The merged model fails to provide structured response. All metrics are reported as `pass@n` scores unless otherwise specified.

Merging Methods	Models	Advanced Reasoning			General Knowledge & Reasoning			Code Gen
		AIME24↑	AIME25↑	GPQA↑	GSM8K↑	BBH↑	MMLU↑	
w/o Merging	Math	90.00	90.00	88.89	97.50	74.37	74.11	87.80
	Code	90.00	86.67	90.40	97.50	87.14	79.97	90.85
Task Arithmetic	Fuse	90.00	83.33	87.37	96.06	86.42	76.77	90.85
Dare Task Arithmetic	Fuse	90.00	86.67	87.37	96.66	86.50	76.69	91.46
Ties Merging	Fuse	90.00	86.67	83.33	96.21	82.74	70.49	93.29
Dare Ties Merging	Fuse	90.00	86.67	88.38	96.13	85.92	75.47	94.51
SCE	Fuse	93.33	83.33	86.36	96.89	83.15	68.64	92.07
SCF-RKL (Ours)	Fuse	90.00	83.33	88.38	97.04	87.72	75.45	92.07

Table 8. Performance of merging Meta-Llama-3-8B-Instruct (Base 0), and MAMmoTH2-8B-Plus(Base 1) on all datasets. \*: The merged model fails to provide structured response. All metrics are reported as `pass@n` scores unless otherwise specified.

Merging Methods	Models	General Knowledge & Reasoning			Code Generation
		GSM8K↑	BBH↑	MMLU↑	
w/o Merging	Base 0	92.72	81.50	66.10	62.80
	Base 1	86.13	76.03	0.00	43.90
Task Arithmetic	Fuse	84.00	83.92	69.10	64.02
Dare Task Arithmetic	Fuse	84.91	84.38	69.31	57.93
Ties Merging	Fuse	21.99	80.47	66.65	69.51
Dare Ties Merging	Fuse	5.69	42.37	61.60	29.27
SCE	Fuse	5.69	39.30	58.52	35.98
SCF-RKL (Ours)	Fuse	91.58	75.64	62.35	51.83

Table 9. Performance of merging Mistral-7B-Instruct-v0.2(Base 0),MathCoder2-Mistral-7B(Base 1) on all datasets. \*: The merged model fails to provide structured response. All metrics are reported as `pass@n` scores unless otherwise specified.

Merging Methods	Models	General Knowledge & Reasoning			Code Generation
		GSM8K↑	BBH↑	MMLU↑	
w/o Merging	Base 0	68.23	66.36	51.99	16.46
	Base 1	45.19	73.03	33.53	0.61
Task Arithmetic	Fuse	78.70	71.61	44.14	39.02
Dare Task Arithmetic	Fuse	79.76	71.38	43.03	39.63
Ties Merging	Fuse	44.35	72.85	33.85	0.00
Dare Ties Merging	Fuse	81.80	75.39	56.09	36.59
SCE	Fuse	43.67	72.41	33.76	0.00
SCF-RKL (Ours)	Fuse	82.79	74.58	56.96	41.46

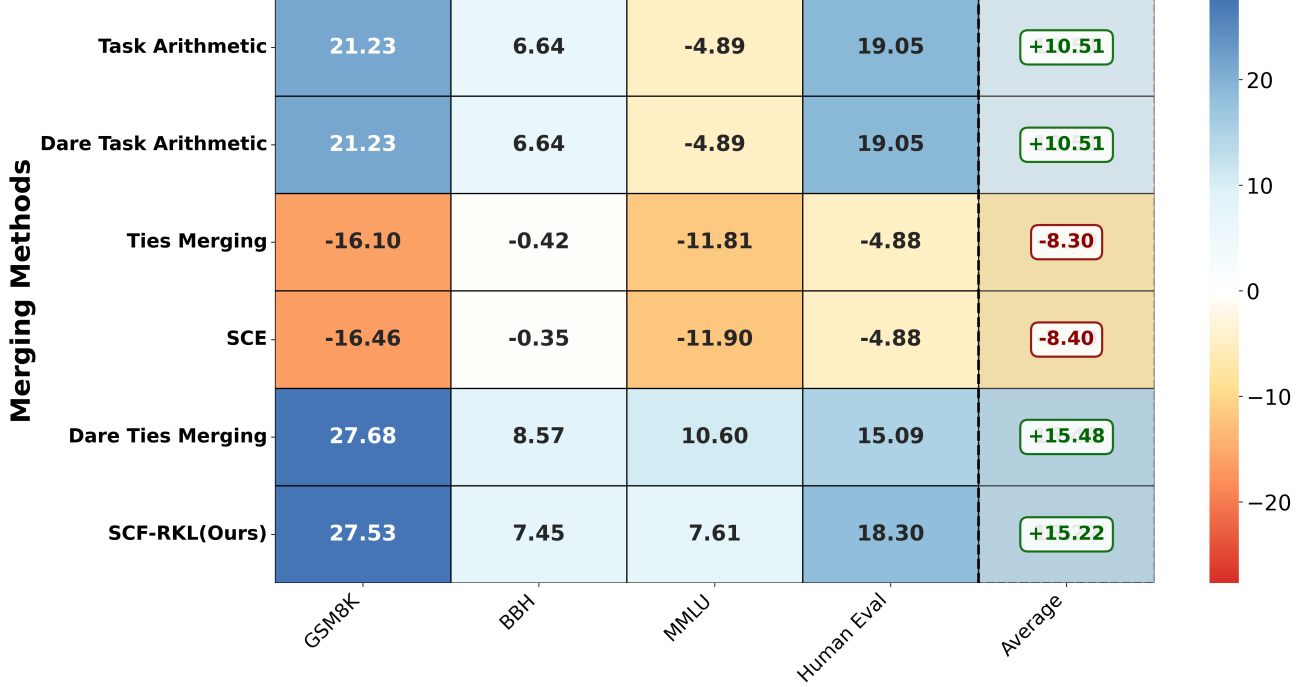


Figure 19. Per-benchmark accuracy change of fused models at the 7B scale, measured as the difference between the fused model’s score and the average score of the two base models. Positive values (blue) indicate improvement; negative values (red) indicate degradation.

Table 10. Performance of merging TinyR1-Preview-Math-32B (Math), and TinyR1-Preview-Science-32B (Sci) on all datasets. All metrics are reported as pass@1 scores.

Methods	Advanced Reasoning				Gen. Know. & Reasoning			Code Gen	Inst. Following		Avg
	AIME 24↑	AIME 25↑	GPQA ↑	LCB ↑	GSM 8K↑	BBH ↑	MMLU ↑	Human Eval↑	IFEval Strict↑	IFBench Strict↑	
w/o Merge	74.6	62.1	68.0	61.7	95.4	48.2	78.1	85.5	63.4	7.8	64.5
	78.0	61.9	68.8	61.5	96.0	61.1	51.7	85.5	60.8	10.2	63.5
SCF-KL	77.6	63.3	68.3	59.1	88.6	61.0	73.8	86.7	58.3	8.7	64.5
SCF-RKL	77.0	62.5	69.2	62.5	95.2	70.3	61.2	86.3	57.9	11.3	65.3

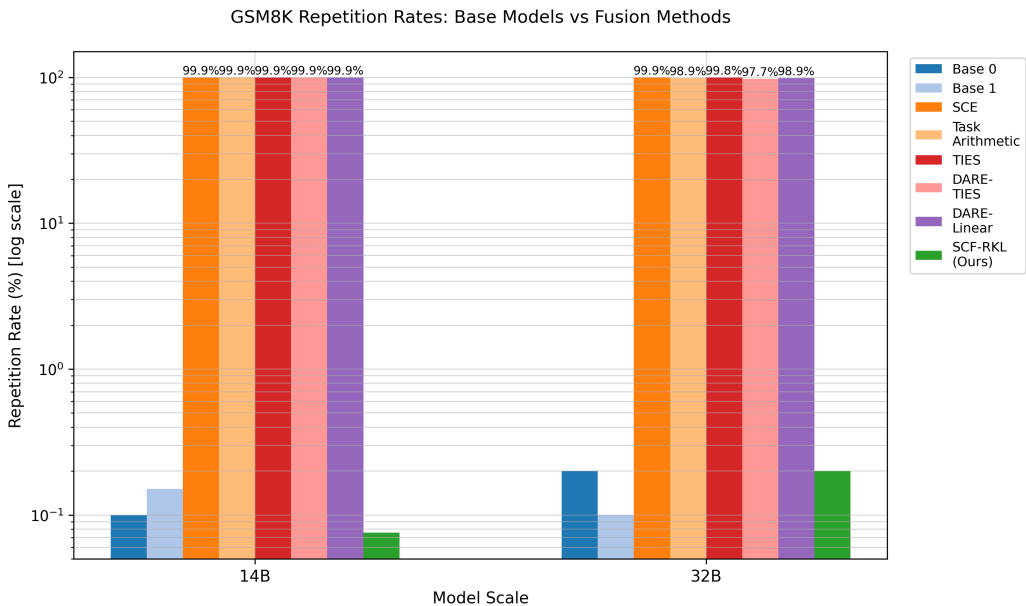


Figure 20. Repetition Rate of models(14B and 32B) on GSM8K

